REVISION

17th July 2014

Oil|Water Interfacial Phosphate Transfer Facilitated by Boronic Acid - Observation of Unusually Fast Oil|Water Lateral Charge Transport

Meng Li [a], Grace E.M. Lewis [a], Tony D. James [a], Yitao Long [b],
Barbara Kasprzyk-Hordern [a], John M. Mitchels [a], and Frank Marken [a]*

[a] *Department of Chemistry, University of Bath, Claverton Down, Bath BA2 7AY (UK)*
[b] *State Key Laboratory of Bioreactor Engineering, Shanghai Key Laboratory of Functional Materials Chemistry & Department of Chemistry, East China University of Science and Technology, Shanghai, 200237 (P. R. China)*

To be submitted to ChemElectroChem

Proofs to F. Marken
Email F.Marken@bath.ac.uk

Abstract

Anion transfer for highly hydrophilic phosphate and hydroxide anions into a water-immiscible organic phase, 3-(4-phenylpropyl)-pyridine (or PPP), is driven with the tetraphenylporphyrinato manganese(II/III) (or TPPMn) redox system and facilitated with a hydrophobic oil-based boronic acid ((3-(1,3-dioxo-6-propylamino-1H-benzo[de]isoquinolin-2(3H)-yl)phenyl)boronic acid). Both, (i) experiments with random arrays of microdroplets (transient) and (ii) experiments in a gold-gold dual-plate oil-filled microtrench generator-collector configuration (approaching steady state), show that phosphate transfer is boronic acid facilitated. At pH 7.5 a switch in mechanism occurs from phosphate transfer to hydroxide transfer. Accelerated charge transport is observed lateral to the oil|water interface. Improved boronic acid facilitators and nano-trench electrodes are discussed in terms of future feasibility for phosphate sensing applications.

Keywords: boronic acid, voltammetry, liquid | liquid interface, phosphate, electroanalysis, micro-trench, sensors.

1. Introduction

Phosphates are ubiquitous in natural waters and important analytical targets for water quality monitoring [1]. Methods for phosphate detection are currently mainly based on colorimetric or conductance probes [2], luminescence probes [3,4,5], fluorescence lifetime [6], poly-amino-phenolic zinc receptors [7], or gravimetric probes [8]. Electrochemical phosphate detection is difficult due to the electrochemically inert and highly hydrophilic nature of phosphate. However, new methods have been reported based on polymer-ferrocene derivatives [9], at zirconia modified screen printed electrodes [10], with molybdate-based sensor films [11], and by voltammetric ion-channel measurements [12].

Electrochemical studies at liquid|liquid interfaces (or at ITIES = Interface of Two Immiscible Electrolyte Solutions [13]) have been reported where facilitated transfer of phosphate was achieved, for example, with calixarene derivatives [14]. A report by Osakai and coworkers [15] demonstrated 20 to 500 μM phosphate detection sensitivity at a liquid|liquid interface with a hexamolybdate heteropolyanion as facilitator for phosphate transfer into the nitrobenzene phase. Whereas traditional liquid|liquid interfacial detection systems require electrolyte in both aqueous and organic phase (this severely limits the range accessible for transfer of highly hydrophilic ions), the development of triple phase boundary ion transfer voltammetry [16] opened up the window to transfer of a wider range of ions. The application of ion transfer voltammetry [17] for the detection of highly hydrophilic anions such as sulphate and chromate [18], carbonate [19], and fluoride [20] has been considered and experimentally realised based on random arrays of oil microdroplets [21]. Similar

triple phase boundary [22] liquid|liquid electrochemical methods have been proposed for the detection of amino acids [23], carboxylates [24], and peptides [25]. A schematic drawing of the process is shown in Figure 1A. The anion A^- transfers across the liquid|liquid phase boundary to maintain charge neutrality upon oxidation of Mn(II) to $Mn(III)^+$.

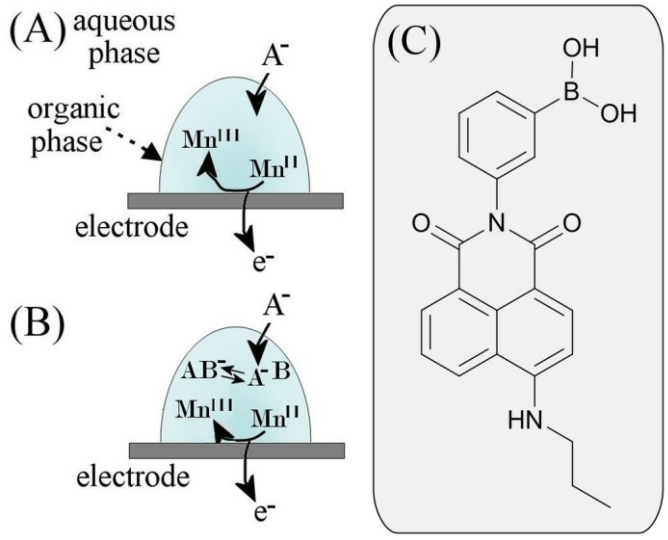

Figure 1. Schematic representation of (A) an oil microdroplet with Mn(III/II) redox system allows anion transfer to be driven by oxidation. (B) In the presence of the facilitator B a complex AB^- is formed to aid anion transfer. (C) Molecular structure of the hydrophobic boronic acid ((3-(1,3-dioxo-6-propylamino-1H-benzo[de]-isoquinolin-2(3H)-yl)phenyl)boronic acid).

Addition of a facilitator, such as a highly hydrophobic boronic acid (see molecular structure in Figure 1C) allows anions to be selected for detection (Figure 1B). This has been demonstrated for example for α-hydroxy-carboxylates such as lactate [26]. Measurements with random arrays of microdroplets are transient (time dependent) in nature and require potential cycling. In order to increase the sensor current and to

introduce steady state (time independent) characteristics, the oil microtrench methodology (see Figure 2) has been introduced [27].

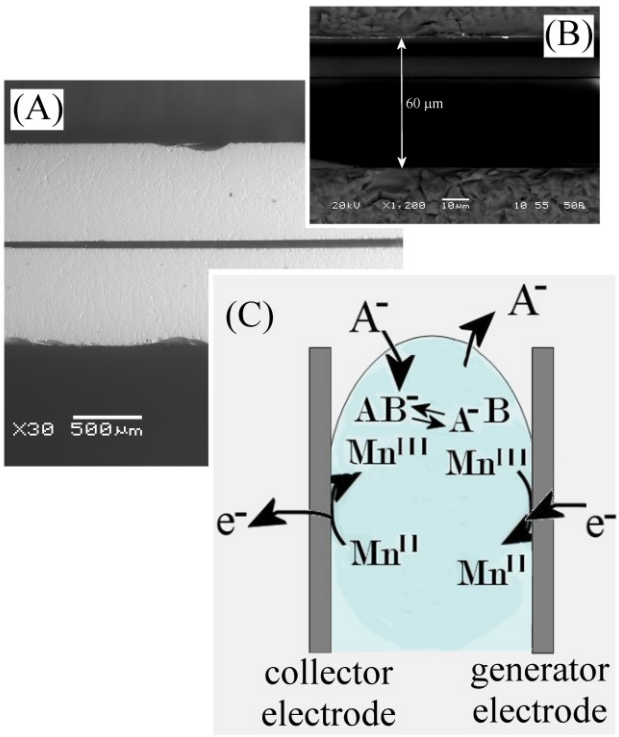

Figure 2. (A) SEM image of the gold-gold dual-plate microtrench electrode. (B) SEM image showing the trench width. (C) Schematic representation of the coupled anode and cathode reaction in generator-collector mode.

By placing the oil microdroplet into the gap between two gold plate electrodes (trench width 60 µm, length 5 mm, and trench depth 300 µm, see Figure 2), the oxidation with coupled anion transfer (collector electrode) can be linked to the corresponding reduction with anion expulsion (generator electrode) back into the aqueous phase (see Figure 2C). For homogeneous redox systems the magnitude of the resulting generator-collector current signal, I_{lim}, is inversely proportional to the inter-electrode gap δ and proportional to the apparent diffusion coefficient D_{app} and the concentration c_0 (equation 1 [28]).

$$I_{\lim} = \frac{FD_{app}Ac_0}{\delta} \quad (1)$$

In this equation F is the Faraday constant, A is the electrode area, and D_{app} is a composite parameter containing contributions from both oxidised and reduced state of the redox system [29] as well as possible contributions from Dahms-Ruff "hopping" of charges [30] at higher concentrations of the redox system (*vide infra*). For a heterogeneous redox system such as an oil microdroplet immobilised in the microtrench additional factors can be important: (i) diffusion down into the trench as opposed to inter-electrode diffusion, (ii) migration contributions due to the absence of supporting electrolyte in the oil phase, (iii) ion "pathway minimisation" effects due to anions entering and leaving in the triple phase boundary reaction zone, (iv) surface effects with accelerated electron hopping and ion transport at the oil|water interface, and (v) Marangoni-type oil|water surface tension driven convection [31].

In this report boronic acid facilitated phosphate transfer is investigated with the aim of exploring novel phosphate sensing protocols. The binding of boronic acid to phosphate after transfer from water to the oil phase is demonstrated to be weak. Information about electronic/ionic transport processes within the oil phase in a microtrench suggests unusually fast transport pathways lateral to the oil|water phase boundary. The mechanism and parameters for future improvements for phosphate detection applications are discussed.

2. Experimental Details

2.1. Chemical Reagents

TPPMn(III)Cl or 5,10,15,20-tetraphenyl-21H,23H-porphine manganese(III) chloride, 4-(3-phenylpropyl)-pyridine, $NaClO_4$, and NaOH were obtained from Aldrich and used without further purification. Demineralised and filtered water was taken from a Vivendi water purification system with not less than 18 MΩ cm resistivity at 22 ^oC.

2.2. Instrumentation

Transient voltammetric experiments were performed on a microAutolab III system (Ecochemie, Netherlands) in staircase voltammetry mode. The step potential was maintained at approximately 1 mV. The counter and reference electrode were platinum gauze and saturated calomel (SCE, Radiometer), respectively. The working electrode was a 4.9 mm diameter basal plane pyrolytic graphite (BPPG, Pyrocarbon, Le Carbon, UK) disc electrode. Steady state voltammetric measurements were performed with a gold-gold dual-plate microtrench electrode [32] and an Autolab PGSTAT30 bipotentiostat. Scanning electron microscopy (SEM) images were obtained on a JEOL SEM6480LV and atomic force microscopy (AFM) was performed with a Veeco Multimode Nanoscope III.

The microtrench electrode was fabricated from gold-coated glass slides assembled with face-to-face with epoxy with dimensions of 5 mm length, 60 μm width (SEM), and ca. 300 μm depth (measured by voltammetry with the $Fe(CN)_6^{3-/4-}$ calibration

redox system [32]). Solutions were de-aerated with argon (BOC). All experiments were conducted at a temperature of 22 +/- 2 ^{o}C.

2.3. Synthesis of (3-(1,3-dioxo-6-(propylamino)-1H-benzo[de]-isoquinolin-2(3H)-yl)phenyl)boronic acid

The boronic acid (see Figure 1C) was synthesized following Heagy's approach [33] by allowing 3-aminophenylboronic acid coupling to 4-bromo-1,8-naphthalic anhydride to give a boronic-naphtalamide derivative. Following Wang's work [34], this derivative was then reacted with propylamine to obtain the target compound. In brief, commercial 4-bromo-1,8-naphthalic anhydride (2.00 g, 7.2 mmol) was dissolved in absolute ethanol (20 mL). An excess of 3-aminobenzeneboronic acid (1.30 g, 8.6 mmol) was added and the mixture was refluxed for 2 h. After the mixture was cooled to room temperature, the precipitate produced was filtered and washed with hexane (3×10 mL) to give a yellow solid (2.57 g, 90% yield), which is the boronic-naphtalamide derivative. Then, this derivative (0.80 g, 2 mmol) and 3 mL propylamine were added into 30 mL of 2-methoxyl ethanol and refluxed for 3 h. After the mixture cooled to room temperature, the solvent was removed under vacuum and the residue was purified with column chromatography (silica gel, DCM–MeOH, 20:1, v/v) to give a yellow solid (0.69 g, 92% yield). ^{1}H NMR (300 MHz, DMSO-d_6, ppm): δ_H 8.77-8.72(m, 1H), 8.43-8.39(m, 1H), 8.26-8.22(m, 1H), 8.13(s, 1H), 7.82(d, J = 7.2 Hz, 1H), 7.72 - 7.62(m, 1H), 7.62 - 7.43(m, 1H), 7.33 - 7.22(m, 1H), 6.79(dd, J_1 = 8.6 Hz, J_2 = 3.3 Hz, 1H), 6.69 - 6.65(m, 1H), 3.40 - 3.35(m, 2H), 1.78 - 1.66(m, 2H), 0.98(t, 3H, J = 7.3Hz). ^{13}C NMR (75 MHz, DMSO-d_6, ppm): δc 164.4, 163.6 158.1, 151.2, 137.8, 136.2, 131.1, 129.7, 128.3, 124.6, 122.6, 120.6, 120.1, 116.6, 115.2,

107.9, 104.2, 44.9, 44.9, 21.5, 11.9. HRMS (ESI) calcd for $C_{21}H_{19}N_2O_4B$ $[M + H]^+$ 375.1516, found 375.154.

2.4. Microdroplet Coatings and Fillings

Solutions of (i) tetraphenylporphinato manganese(III) chloride MnTPPCl or (ii) boronic acid and 4-(3-phenylpropyl)-pyridine (PPP) in acetonitrile were prepared with typically 4 mg MnTPPCl/boronic acid and 80 mg PPP in 10 mL of acetonitrile. A volume of 5-10 μL of mixed solutions (i) and (ii) was then transferred onto the basal plane pyrolytic graphite surface. Following acetonitrile evaporation a microdroplet deposit of approximately 80 nL PPP containing MnTPPCl and boronic acid was obtained. Microtrench filling was achieved by repeated evaporation of acetonitrile solution and gently wiping off excess organic phase from the microtrench surface.

In order to ensure liquid-like behaviour, droplet deposits of the PPP solution of boronic acid were studied by AFM micro-rheology (see Figure 3). The primary resonance of an AFM probe in air was observed at 337 kHz and when immersed into the liquid microdroplet this shifted down by up to 100 kHz (with considerable variations due to droplet size and probe positioning within the microdroplet). Importantly, in all cases liquid-like behaviour was observed and the dimensionless quality factor (Q = defined here as resonance frequency / resonance line width at half height) for the fundamental probe resonance shows a monotonic trend (see Figure 3) towards broader peaks. This is consistent, at least qualitatively, with an increase in viscosity with higher boronic acid concentration [35].

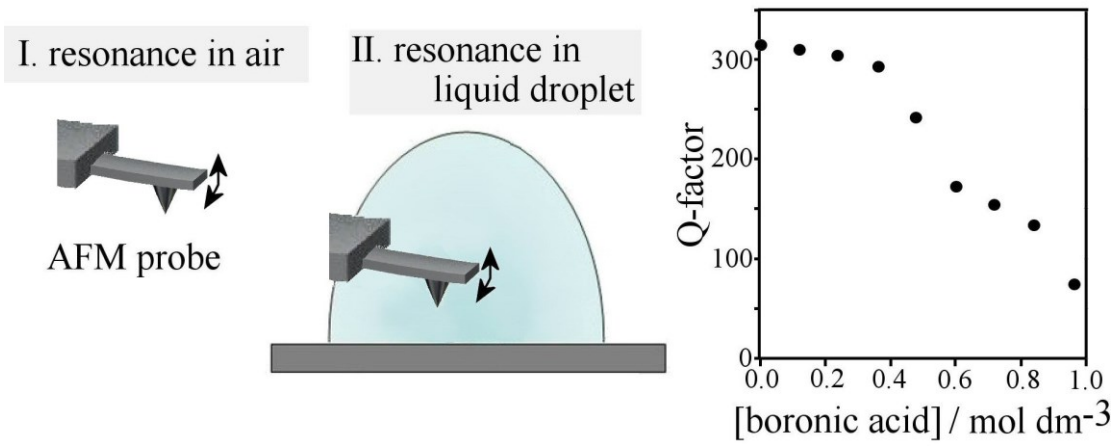

Figure 3. Schematic drawing of the AFM probe resonating in air and immersed into liquid microdroplet. Plot of the quality factor versus concentration of boronic acid in a PPP microdroplet.

3. Results and Discussion

3.1. The Effect of Boronic Acid on the Transfer of Phosphate Anions I.: Transient Voltammetry

MnTPP immobilised in PPP solvent microdroplets onto graphite and immersed into aqueous 0.1 M NaH_2PO_4 (pH 4.5, see Figure 4A) exhibits a well-defined reduction and back-oxidation signal with midpoint potential (calculated from peak potentials as E_{mid} = 0.5 $E_{p,red}$ + 0.5 $E_{p,ox}$) of 0.11 V vs. SCE. This process is associated with the transfer of an anion (here probably $H_2PO_4^-$) into the oil phase to maintain charge neutrality.

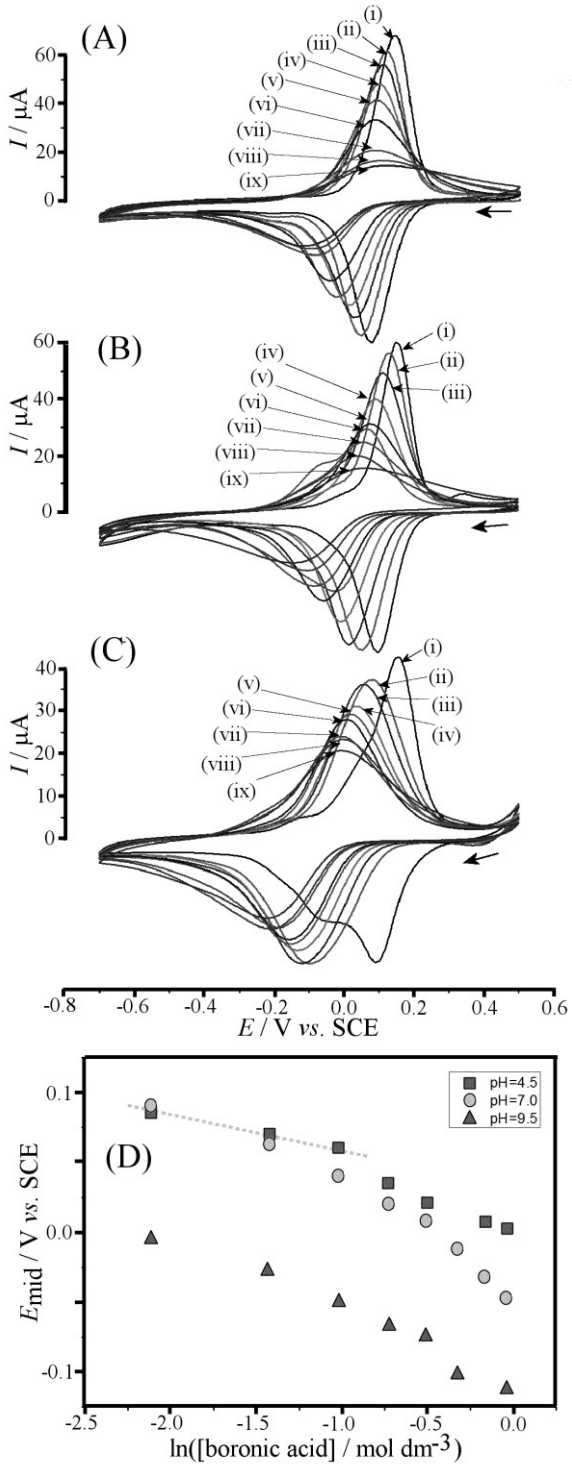

Figure 4. (A) Cyclic voltammograms (scan rate 50 mV s^{-1}) for 56 mM TPPMn in PPP on graphite immersed in 0.1 M NaH_2PO_4 pH 4.5 with (i) 0.0, (ii) 0.12, (iii) 0.24, (iv) 0.36, (v) 0.48, (vi) 0.60, (vii) 0.72, (viii) 0.84, (ix) 0.96 M boronic acid. (B) As above, but at pH 7.0. (C) As above, but in 0.1 M Na_2HPO_4 pH 9.5. (D) Plot of E_{mid} potentials *versus* boronic acid concentrations for pH= 4.5, 7.0, 9.5. The dashed line indicates the theoretical trend for a binding constant K = 20 mol^{-1} dm^3 (see text).

Addition of boronic acid leads to lowered peak currents and broadening of the voltammetric response as well as a shift of midpoint potential E_{mid} to more negative values. This characteristic shift in E_{mid} is indicative of easier oxidation/anion transfer due to the facilitation effect with the boronic acid complexing the anion in the organic phase. A plot is shown in Figure 4D. The overall reaction based on a 1:1 phosphate : boronic acid complex is assumed here tentatively (equation 2).

$$Mn(II)(oil) + B(oil) + A^-(aq) \rightleftharpoons Mn(III)^+(oil) + AB^-(oil) \qquad (2)$$

The theoretical model for this complexation [26] suggests an estimated binding constant of $K = \frac{[AB^-(oil)]}{[A^-(oil)][B(oil)]}$ = 20 mol^{-1} dm^3 (see dashed line in Figure 4D) consistent with relatively weak binding [26]. At higher boronic acid concentrations ([boronic acid] > 0.6 mol dm^{-3}) stronger binding is observed (see trend in E_{mid} values), which is likely to be associated with 1:2 phosphate to boronic acid complexation.

Experiments performed at pH 7 show a similar trend (Figure 4B) with clear boronic acid facilitation effects. The plot in Figure 4D confirm transfer of phosphate according to equation 2, however, the increase in deviation at higher boronic acid concentration suggests further 1:2 phosphate to boronic acid complexation (this process is pH dependent). Perhaps interestingly, at pH 9.5 the characteristics of the system change. Although a similar set of voltammograms is obtained (Figure 4C), the plot of midpoint potentials (Figure 4D) now is shifted negative, whilst still implying complexation by boronic acid. In order to further investigate this effect, experiments

were performed at fixed boronic acid concentration (0.36 M) but with varying pH (Figure 5).

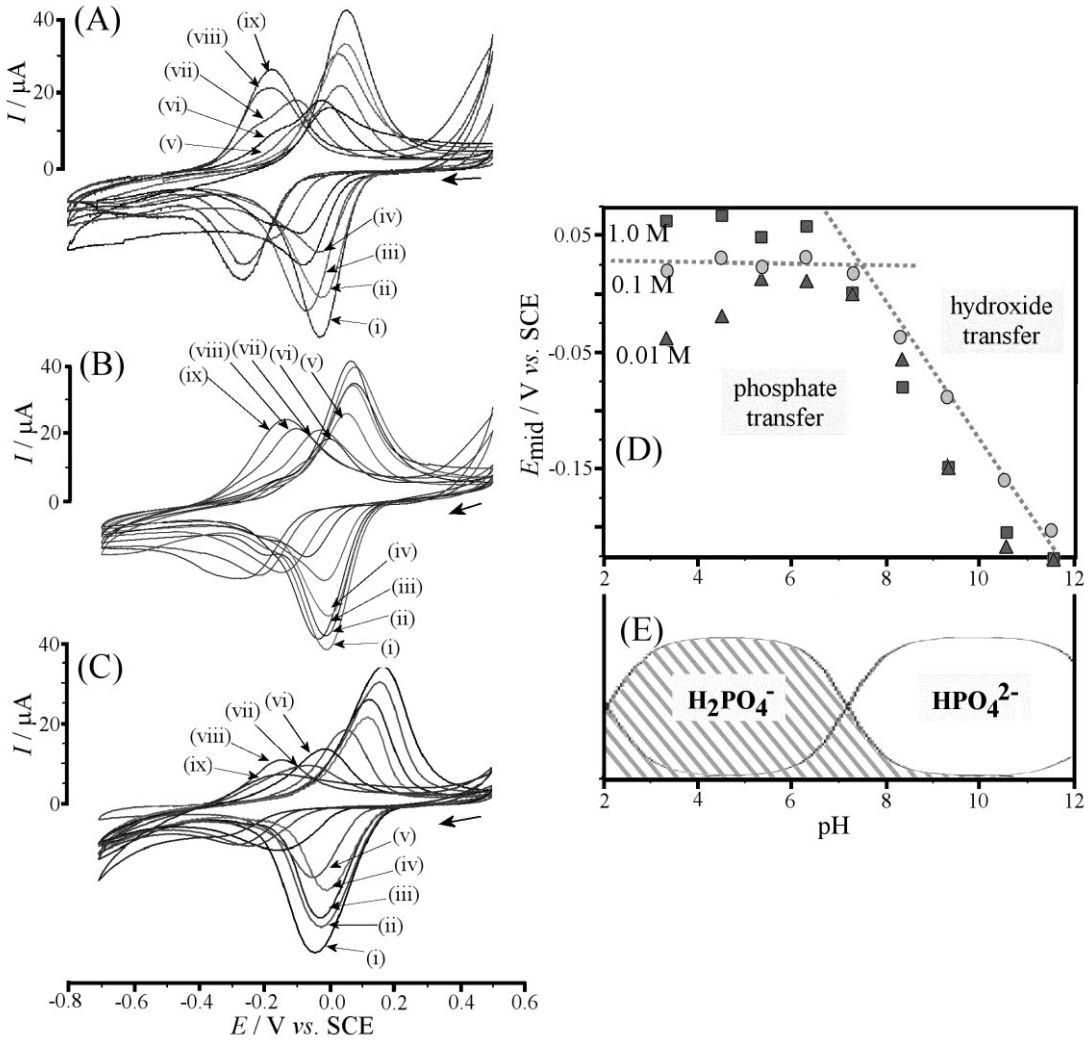

Figure 5. (A) Cyclic voltammograms (scan rate 50 mV s^{-1}) for 64 mM TPPMn with 0.36 M boronic acid in PPP on graphite immersed in 1.0 M phosphate buffer at pH = (i) 3.4, (ii) 4.2, (iii) 5.3, (iv) 6.2, (v) 7.2, (vi) 8.3, (vii) 9.3, (viii) 10.5, (ix) 11.5. (B) As before for 0.1 M phosphate buffer. (C) As before for 0.01 M phosphate buffer. (D) Plot of E_{mid} potentials *versus* pH. (E) Speciation plot.

These experiments were performed for 1.0 M, 0.1 M, and 0.01 M phosphate buffer and generally similar trends are observed (Figure 5A-C). In the acidic pH range well-defined reversible peaks are indicative of phosphate anion transfer (with an increase in peak-to-peak separation at lower supporting electrolyte concentration). However, in

the alkaline pH range, a smaller somewhat broader peak response is detected (with a decrease in peak current at lower supporting electrolyte concentration). The E_{mid} for the process in the alkaline pH-range appears pH-dependent. From the plot of E_{mid} values versus pH (Figure 5D) a switch in mechanism is observed at pH 7.5. In the acidic pH range a constant value consistent with phosphate transfer (that is transfer of $H_2PO_4^-$, see Figure 5E, see equation 2) is observed, but in the alkaline pH range a Nernstian slope of approximately -59 mV pH^{-1} suggests the transfer of either protons (expulsion) or hydroxide (uptake) during oxidation of MnTPP. The net process is here formally (based on the knowledge that hydroxide can bind to boronic acids) assigned here to hydroxide uptake rather than proton expulsion (equation 3). However, contributions from proton expulsion could also be possible upon dissociation of water within the organic phase and it could explain the observed change in peak shape.

$$Mn(II)(oil) + B(oil) + OH^-(aq) \rightleftharpoons Mn(III)^+(oil) + HOB^-(oil) \qquad (3)$$

When systematically varying the phosphate buffer concentration also a close to Nernstian E_{mid} shift of approximately 50 mV is observed (see Figure 5D at pH 3.4) consistent with the phosphate transfer process suggested in equation 2. It is interesting to extrapolate the hydroxide concentration to 0.1 M (pH 11) to obtain the potential difference for transfer of $H_2PO_4^-$ versus transfer of hydroxide as ca. ΔE = 0.2 V. This potential difference is here composed of predominantly two components: (i) the difference in hydration energy of $H_2PO_4^-$ versus OH^- in water and (ii) the difference in binding constant to the boronic acid in the oil phase.

3.2. The Effect of Boronic Acid on the Transfer of Phosphate Anions II.: Steady State Voltammetry

In order to obtain further information about the mechanism of phosphate transfer and to explore steady state conditions for sensing, an oil microtrench experiment is conducted. The gold-gold dual-plate microtrench of ca. 60 μm width, 5 mm length, and ca. 300 μm depth is filled with oil phase (ca. 90 nL) and immersed into aqueous solution. One of the electrodes is at fixed potential ($E_{collector}$ = 0.5 V vs. SCE) and the second electrode potential is scanning ($E_{generator}$). Figure 6A shows typical generator (reduction) and collector (oxidation) voltammograms consistent with coupled anion uptake and anion expulsion.

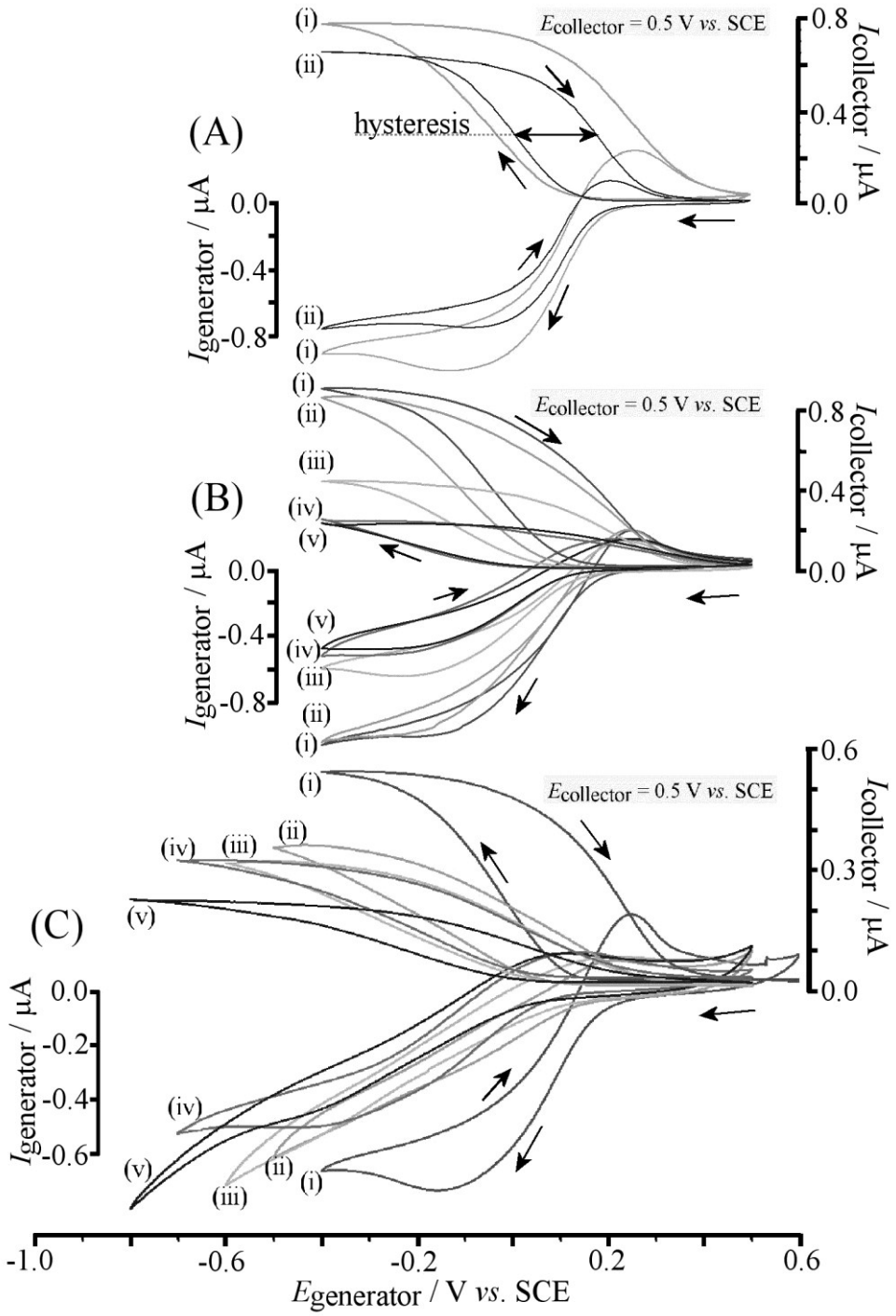

Figure 6. (A) Generator and collector currents for cyclic voltammograms (scan rate (i) 20 mV s^{-1} and (ii) 10 mV s^{-1}) for 65 mM TPPMn in PPP in a microtrench immersed in 0.1 M NaH_2PO_4 pH 4.5. The collector hysteresis effect is indicated. (B) Generator and collector currents for cyclic voltammograms (scan rate 10 mV s^{-1}) for 65 mM TPPMn in PPP immersed in 0.1 M NaH_2PO_4 pH 4.5 with (i) 0.0, (ii) 0.19, (iii) 0.37, (iv) 0.56, (v) 0.75 M boronic acid. (C) As before, but at pH 9.5.

The magnitude of the mass transport controlled limiting current is indicative of rapid diffusion of Mn(III) from the collector to the generator and of Mn(II) diffusion back. An interesting parameter in this kind of electrode system is the collector current hysteresis ΔE_H, which is indicated in Figure 6A. The apparent rate of diffusion is linked (approximately) to this parameter via equation 4 [36].

$$\Delta E_H = 0.0071 \times \frac{v\delta^2 F}{D_{app} RT} \qquad (4)$$

In this equation ΔE_H is given by the scan rate v, the inter-electrode gap δ, the Faraday constant F, that apparent diffusion coefficient D_{app}, the gas constant R, and the absolute temperature T. In Figure 6A it can be seen that doubling the scan rate does double the hysteresis as expected. For a typical ΔE_H = 0.1 V (see Figure 6A) the apparent diffusion coefficient can be estimated as $D_{app} = 10^{-10}$ m^2 s^{-1}. This seems surprisingly high given the viscous nature of the oil phase and the size of molecular species involved. The value is likely to be at least in part indicative of contributions from transport mechanisms other than conventional diffusion in the oil phase. But also the *pathway* of charge transport could be important here (*vide infra*). With D_{app} estimated, it is possible to calculate the "active depth" of the microtrench based on equation 1. The calculated value, 13 μm, is very low and likely to imply that only a thin layer of oil at the top of the microtrench (close to the triple phase boundary reaction zone and close to the oil|water interface) is active for the anion/electron transport. Deeper regions within the microtrench appear to be ineffective during charge transport possibly due to the extended pathway length away from the triple phase boundary reaction zone.

When comparing data in Figure 6B (pH 4.5) and 6C (pH 9.5) it can be seen that the phosphate transfer is associated with (i) a higher hysteresis (somewhat slower diffusion) and (ii) similar limiting currents when compared to hydroxide transfer. The increase in hysteresis and decrease in limiting currents observed for the collector currents in Figure 6B when boronic acid is added into the oil phase is believed to be linked to the increase in viscosity (compare the decrease in peak current and shape in Figure 4A). Perhaps surprisingly, for the hydroxide transfer the limiting current decreases with boronic acid addition, but the collector current hysteresis appears to remain almost constant. This could be associated with a smaller change in D_{app} and/or a change in reaction layer depth.

The observation of rapid diffusion of the redox system and bound anions close to the oil|water interface is tantalising and a sign of a preferred pathway and/or additional transport mechanisms. Accumulation of MnTPP(II/III) close to the oil|water interface and reversible binding to boronic acid close to the interface may be factors in the overall process. For an adsorbed layer of MnTPP(II/III) at the liquid|liquid interface Dahms-Ruff type charge hopping could be possible [37,38]. For this case the apparent diffusion coefficient would be given as $D_{app} = D_{phys} + \pi(k \times \delta^2)/4$ where D_{phys} is the physical diffusion coefficient, k is the concentration dependent hopping rate with average intermolecular hopping distance δ. To account for $D_{app} = 10^{-10}$ m^2s^{-1} the rate constant k (and therefore the concentration) would have to be very high.

An alternative and perhaps also plausible explanation for the unusually fast transport of charges at the oil|water interface between generator and collector could be based on

surface tension driven (Marangoni) convection [31]. A convective loop in the oil phase could cause a flow of redox active material between generator and collector electrodes, thereby effectively recycling the redox system. Experimental observations from microtrench experiments therefore suggest complexity and unresolved mechanistic and transport questions. However, the feasibility of steady state phosphate ion transfer detection (at high phosphate concentration and at low pH) has been demonstrated.

5. Conclusions

Ion transfer voltammetry for phosphate, $H_2PO_4^-$, has been demonstrated with details of the mechanism, transport, and speciation not fully resolved. Relatively weak binding of a boronic acid to phosphate is suggested with a switch from phosphate transfer to hydroxide transfer already at $[OH^-]/[H_2PO_4^-] = 10^{-7.5}/0.05 = 6 \times 10^{-7}$. The facilitated transfer of hydroxide appears therefore much preferred. In order to further develop this methodology the following issues need to be addressed:

- The binding of boronic acid to phosphate needs to be much stronger and specific possibly with a custom-synthesised multi-dentate boronic acid
- For sensing applications the design of the microtrench electrode system needs to be improved with smaller gap (nano-gap) and long-term water resistant stationary oil phase. In particular the smaller gap will increase the sensor current and further decrease the time constant for inter-electrode transport
- The effect of the concentration of phosphate then needs to be investigated as a parameter in the anion transfer and transport profile in the microtrench. With

faster transport phosphate concentration variations should be associated with a systematic change in the limiting current

- The speciation and effects of potential interferences need to be investigated and optimised

In spite of the issues that remain to be addressed, this study provides a first proof-of-principle demonstration of a phosphate concentration dependent liquid|liquid anion transfer process made selective with a boronic acid facilitator and amplified in a steady state sensing configuration employing an oil-filled microtrench. Most interestingly, the interfacial oil|water transport of charge is considerably faster than expected based on viscosity and molecular diffusion.

Acknowledgement

M.L. is grateful for financial support from the China Scholarship Council (CSC) and a University of Bath Scholarship. G.E.M.L. thanks NERC (NE/1019456/1) for funding.

References

[1] C. Warwick, A. Guerreiro, A. Soares, *Biosens. Bioelectronics*, **2013**, *41*, 1-11.

[2] C. Warwick, A. Guerreiro, A. Gomez-Caballero, E. Wood, J. Kitson, J. Robinson, A. Soares, *Biosens. Bioelectronics*, **2014**, *52*, 173-179.

[3] J.M. Bai, L. Zhang, R.P. Liang, J.D. Qiu, *Chem. Europ. J*. **2013**, *19*, 3822-3826.

[4] Z.B. Zheng, Y.Q. Wu, K.Z. Wang, F.Y. Li, *Dalton Trans.* **2014**, *43*, 3273-3284.

[5] J. Massue, S.J. Quinn, T. Gunnlaugsson, *J. Amer. Chem. Soc*. **2008**, *130*, 6900-6901.

[6] J.M. Paredes, M.D. Giron, M.J. Ruedas-Rama, A. Orte, L. Crovetto, E.M. Talavera, R. Salto, J.M. Alvarez-Pez, *J. Phys. Chem. B* **2013**, *117*, 8143-8149.

[7] G. Ambrosi, M. Formica, V. Fusi, L. Giorgi, A. Guerri, E. Macedi, M. Micheloni, P. Paoli, R. Pontellini, P. Rossi, *Inorg. Chem*. **2009**, *48*, 5901-5912.

[8] J.M.M. Rodrigues, A.S.F. Farinha, P.V. Muteto, S.M. Woranovicz-Barreira, F.A.A. Paz, M.G.P.M.S. Neves, J.A.S. Cavaleiro, A.C. Tome, M.T.S.R. Gomes, J.L. Sessler, *Chem. Commun.* **2014**, *50*, 1359-1361.

[9] O. Karagollu, M. Gorur, F. Gode, B. Sennik, F. Yilmaz, *Sens. Actuators B-Chem*. **2014**, *193*, 788-798.

[10] W.L. Cheng, J.L. Chang, Y.L. Su, J.M. Zen, *Electroanalysis* **2013**, *25*, 2605-2612.

[11] S. Berchmans, R. Karthikeyan, S. Gupta, G.E.J. Poinern, T.B. Issa, P. Singh, *Sens. Actuators B-Chem.* **2011**, *160*, 1224-1231.

[12] H. Aoki, K. Hasegawa, K. Tohda, Y. Umezawa, *Biosens. Bioelectronics* **2003**, *18*, 261-267.

[13] H.H.J. Girault, D.J. Schiffrin, *Electroanal. Chem.* **1989**, *15*, 1-141.

[14] F. Kivlehan, W.J. Mace, H.A. Moynihan, D.W.M. Arrigan, *Electrochim. Acta* **2009**, *54*, 1919-1924.

[15] T. Osakai, S. Himeno, A. Saito, H. Katano, *Electroanalysis* **1993**, *5*, 215-219.

[16] F. Scholz, U. Schröder, R. Gulaboski, *Electrochemistry of Immobilized Particles and Droplets*, Springer, Berlin, **2005**.

[17] M.J. Bonné, C. Reynolds, S. Yates, G. Shul, J. Niedziolka, M. Opallo, F. Marken, *New J. Chem.* **2006**, *30*, 327-334.

[18] F. Marken, C.M. Hayman, P.C.B. Page, *Electroanalysis*, **2002**, *14*, 172-176.

[19] A.M. Collins, J.D. Watkins, N. Katif, Y.J. Huang, Y.B. Jiang, T.D. James, S.D. Bull, F. Marken, *Chem. Commun.* **2011**, *47*, 12002-12003.

[20] A.M. Collins, G.J. Blanchard, F. Marken, *Electroanalysis*, **2012**, *24*, 246-253.

[21] F. Marken, R.D. Webster, S.D. Bull, S.G. Davies. *J. Electroanal. Chem*. **1997**, *437*, 209-218.

[22] C.E. Banks, T.J. Davies, R.G. Evans, G. Hignett, A.J. Wain, N.S. Lawrence, J.D. Wadhawan, F. Marken, Compton, R.G., *Phys. Chem. Chem. Phys*. **2003**, *5*, 4053-4069.

[23] R. Gulaboski, V. Mirceski, F. Scholz, *Amino Acids*, **2003**, *24*, 149-154.

[24] S.M. MacDonald, M. Opallo, A. Klamt, F. Eckert, F. Marken, *Phys. Chem. Chem. Phys.* **2008**, *10*, 3925-3933.

[25] R. Gulaboski, F. Scholz, *J. Phys. Chem. B*, **2003**, *107*, 5650-5657.

[26] N. Katif, R.A. Harries, A.M. Kelly, J.S. Fossey, T.D. James, F. Marken, *J. Solid State Electrochem.* **2009**, *13*, 1475-1482.

[27] S.E.C. Dale, Y.H. Chan, P.C.B. Page, E.O. Barnes, R.G. Compton, F. Marken, *Electrophorsis*, **2013**, *34*, 1979-1984.

[28] S.E.C. Dale, C.E. Hotchen, F. Marken, *Electrochim. Acta* **2013**, *101*, 196-200.

[29] S.E.C. Dale, A. Vuorema, M. Sillanpää, J. Weber, A.J. Wain, E.O. Barnes, R.G. Compton, F. Marken, *Electrochim. Acta,* **2014**, *125*, 94-99.

[30] C.Y. Cummings, J.D. Wadhawan, T. Nakabayashi, M. Haga, L. Rassaei, S.E.C. Dale, S. Bending, M. Pumera, S.C. Parker, F. Marken, *J. Electroanal. Chem*. **2011**, *657*, 196-201.

[31] J.C. Ball, F. Marken, F.L. Qiu, J.D. Wadhawan, A.N. Blythe, U. Schröder, R.G. Compton, S.D. Bull, S.G. Davies, *Electroanalysis* **2000**, *12*, 1017-1025.

[32] S.E.C. Dale, F. Marken, *Faraday Discuss*. 2013, **164**, 349-359.

[33] H. Cao, D. I. Diaz, N. DiCesare, J. R. Lakowicz, M. D. Heagy, *Org. Lett.*, **2002**, *4*, 1503-1505.

[34] Z. Chen, L. Wang, G. Zou, X. Cao, Y. Wu, P. Hu, *Spectrochim. Acta A: Mol. Biomol. Spectroscopy*, **2013**, *114*, 323-329.

[35] M. Hennemeyer, S. Burghardt, R.W. Stark, *Sensors*, **2008**, *8*, 10-22.

[36] A. Vuorema, H. Meadows, N. Bin Ibrahim, J. Del Campo, M. Cortina-Puig, M.Y. Vagin, A.A. Karyakin, M. Sillanpää, F. Marken, *Electroanalysis*, **2010**, *22*, 2889-2896.

[37] H. Dahms, *J. Phys. Chem.* **1968**, *72*, 362-363.

[38] I. Ruff, V.J. Friedrich, *J. Phys. Chem.* **1971**, *75*, 3297-3302.